

Cite this: *Chem. Sci.*, 2024, 15, 18896

All publication charges for this article have been paid for by the Royal Society of Chemistry

Received 7th May 2024
Accepted 5th October 2024

DOI: 10.1039/d4sc02995j

rsc.li/chemical-science

Quantitative analysis of air-oxidation reactions of thiolate-protected gold nanoclusters†

Wataru Suzuki,^{‡a} Ryo Takahata,^{‡ab} Yoshiyuki Mizuhata,^{‡abc}
Norihiro Tokitoh,^{‡abc} Songlin Xue^{‡d} and Toshiharu Teranishi^{‡*ab}

The interaction of dioxygen (O₂) with inorganic nanomaterials is one of the most essential steps to understanding the reaction mechanism of O₂-related reactions. However, quantitative analyses for O₂-binding processes and subsequent oxidation reactions on the surface are still elusive, whereas the reaction of O₂ with molecules such as transition metal complexes has been widely explored. Herein, we have quantitatively evaluated reaction processes of air-oxidation reactions of atomically precise thiolate-protected Au₂₅ nanoclusters ([Au₂₅(SR)₁₈][−]) as a model of O₂ activation by inorganic nanomaterials. Kinetic analyses on the air-oxidation reaction of [Au₂₅(SR)₁₈][−] revealed a controlling factor for O₂-activation processes, which could be finely tunable by the protecting thiolate ligands.

Introduction

Dioxygen (O₂) activation in O₂ reduction and aerobic oxidations is one of the most fundamental and crucial reaction processes in chemistry. So far, many catalysts for O₂ activation have been developed by employing molecular catalysts^{1–3} and inorganic nanomaterials, including metal nanoparticles (MNPs)^{4–6} and metal nanoclusters (MNCs).^{7–9} An understanding of the reaction mechanisms of O₂-activation processes at the atomic level is essential to develop more efficient catalysts. Hence, mechanistic insights into O₂ activation have also been investigated.^{10–13} For molecular catalysts such as Fe, Co and Cu complexes or organocatalysts such as porphyrinoids, O₂-activation processes, including O₂-binding and subsequent reduction to form reactive O₂ species, were experimentally well-revealed through structural¹⁰ and kinetic¹¹ analyses based on experimental evidence. In contrast, because reaction systems with MNPs are relatively complicated due to the distributions of size and composition of MNPs, the understanding of the reaction mechanisms for the O₂-activation process at the atomic level is quite a difficult challenge. Thus, estimations of such a reaction mechanism have mainly relied on theoretical analysis until now.¹²

Compared with MNPs, MNCs with sizes of less than 2 nm are considered a desirable model to reveal detailed reaction mechanisms at the atomic level owing to their atomically precise structures.¹⁴ Among various MNCs, gold nanoclusters (AuNCs), such as thiolate-protected gold clusters (denoted as Au_n(SR)_m, SR = thiolate), are appropriate candidates to perform atomically precise analyses on O₂-activation processes using inorganic nanomaterials because of their tunable reactivities, easy preparation and good stability.^{7,15,16} For example, the thiolate-protected Au₂₅ cluster anion ([Au₂₅(SR)₁₈][−]) exhibited reactivity towards O₂, as seen in the catalytic oxygen reduction reaction (ORR).¹⁷ The catalytic activity of [Au₂₅(SR)₁₈][−] in the ORR could be tuned by the type of thiolate ligand^{17a} and heteroatom doping.^{17b} In addition, [Au₂₅(SR)₁₈][−] which shows higher reactivity than other AuNCs with different sizes^{17c} is a promising material for practical use. Together with the ORR, the reactions of [Au₂₅(SR)₁₈][−] with O₂ are also important in the reductive activation of O₂ for substrate oxidation, which was seen in the aerobic oxidation of thiols to form disulfide in Au₂₅ polymer films.¹⁸ In both cases, the interaction of O₂ on the surface of the Au₂₅ cluster and reduction of O₂, namely Au₂₅ cluster oxidation,^{19,20} are proposed to be crucial processes as an initial step for O₂ activation. However, whereas some reports demonstrated the interaction between O₂ and [Au₂₅(SR)₁₈][−] using mass spectrometry²¹ or theoretical analysis,^{13d,f,17d} experimental evidence for the O₂ binding and/or activation by AuNCs is still limited. In particular, the air-oxidation reaction of [Au₂₅(SR)₁₈][−] was analysed just qualitatively,²² but quantitative analysis for O₂ activation by AuNCs, which is important to systematically evaluate the reactivities of AuNCs, has yet to be reported.

Herein, we report quantitative analyses of the air-oxidation reactions of AuNCs based on kinetic analysis for the first time. For a model of AuNCs, we chose [Au₂₅(SR)₁₈][−] because of

^aInstitute for Chemical Research, Kyoto University, Uji, Kyoto, 611-0011, Japan. E-mail: teranishi@scl.kyoto-u.ac.jp

^bGraduate School for Science, Kyoto University, Uji, Kyoto, 611-0011, Japan

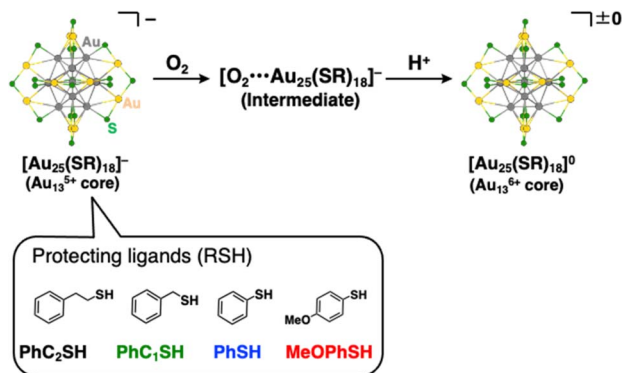
^cIntegrated Research Consortium on Chemical Sciences, Uji, Kyoto, 611-0011, Japan

^dSchool of Chemistry and Chemical Engineering, Jiangsu University, 301 Xuefu Road, Zhenjiang 212013, China

† Electronic supplementary information (ESI) available. CCDC 2299526. For ESI and crystallographic data in CIF or other electronic format see DOI: <https://doi.org/10.1039/d4sc02995j>

‡ Present Address: University of Hyogo, Himeji, 671-2280, Japan.





Scheme 1 Reaction scheme for air-oxidation reactions of $[\text{Au}_{25}(\text{SR})_{18}]^-$ employed in this work. R groups were omitted for clarity. Atom labels: grey: gold in the Au_{13} core, yellow: gold on the staple, and green: sulfur.

its reversible redox properties²⁰ and a variety of choices for protecting ligands.^{14,23} The Au_{25} cluster anions are composed of an Au_{13}^{5+} core surrounded by six $[\text{Au}_2(\text{SR})_3]^-$ units, and the oxidation reactions of the gold cluster occur in the Au_{13} core rather than in staple moieties.^{19b} Evaluations of the reactivities of $[\text{Au}_{25}(\text{SR})_{18}]^-$ with O_2 were conducted in the presence of protons (Scheme 1). The addition of protons can promote the electron transfer reaction to reduce O_2 through proton-coupled electron transfer (PCET)²⁴ and this reaction system has a big advantage of facile quantitative analysis of the reactivity, as seen in the mechanistic analysis of O_2 reduction by organic molecules^{3c,25} or transition metal complexes.²⁶ We have controlled redox potentials and O_2 -affinities of $[\text{Au}_{25}(\text{SR})_{18}]^-$ by changing the thiolate (SR) ligands and revealed controlling factors in air-oxidation reactions of $[\text{Au}_{25}(\text{SR})_{18}]^-$ to form neutral $[\text{Au}_{25}(\text{SR})_{18}]^0$.

Results and discussion

Synthesis and characterisation of thiolate-protected Au_{25} cluster anions

Synthesis of the phenylethanethiolate-protected Au_{25} cluster anion ($\text{TOA}^+[\text{Au}_{25}(\text{SC}_2\text{Ph})_{18}]^-$, TOA^+ = tetraoctylammonium) was conducted through the reduction of Au(I)-thiolate complexes according to the previous report.²⁷ Other Au_{25} clusters ($\text{TOA}^+[\text{Au}_{25}(\text{SR})_{18}]^-$) with different thiolate ligands (phenylmethanethiol (PhC_1SH), thiophenol (PhSH) and 4-methoxythiophenol (MeOPhSH)) were synthesized using ligand-exchange reactions. Phenylmethanethiolate-protected Au_{25} cluster anions ($\text{TOA}^+[\text{Au}_{25}(\text{SC}_1\text{Ph})_{18}]^-$) were successfully synthesized through the ligand-exchange reaction of $\text{TOA}^+[\text{Au}_{25}(\text{SC}_2\text{Ph})_{18}]^-$ with excess amounts of PhC_1SH in CH_2Cl_2 . $\text{TOA}^+[\text{Au}_{25}(\text{SPh})_{18}]^-$ and $\text{TOA}^+[\text{Au}_{25}(\text{SPhOMe})_{18}]^-$ were prepared by the ligand-exchange reaction of the cyclohexanethiolate-protected Au_{23} cluster ($\text{TOA}^+[\text{Au}_{23}(\text{SCy})_{16}]^-$, SCy = cyclohexanethiolate) with PhSH or MeOPhSH (see the ESI† for detailed synthetic methods).²⁸ A series of thiolate-protected Au_{25} cluster anions were characterised using UV-vis absorption spectroscopy, ^1H NMR, ESI-MS and X-ray

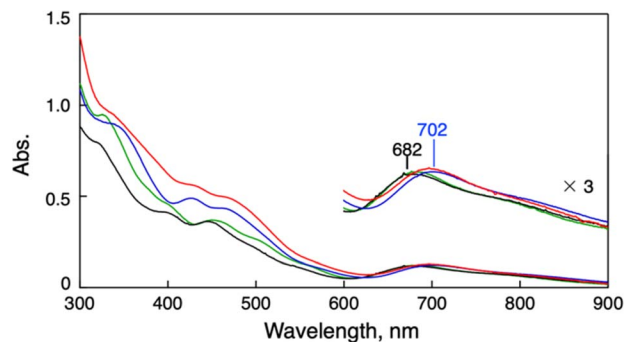


Fig. 1 UV-vis spectra of $\text{TOA}^+[\text{Au}_{25}(\text{SR})_{18}]^-$ (0.010 mM) in THF. SR = SC_2Ph (black), SC_1Ph (green), SPh (blue) and SPhOMe (red).

absorption fine structure (XAFS) measurements (Fig. 1 and S1–S6†). In negative-mode ESI-MS spectra (Fig. S1†) of $\text{TOA}^+[\text{Au}_{25}(\text{SR})_{18}]^-$, peaks from $[\text{Au}_{25}(\text{SR})_{18}]^-$ were clearly observed as well as the results of ^1H NMR spectroscopy (Fig. S2–S5†), supporting the high purity of the products. UV-vis absorption spectra of all products in tetrahydrofuran (THF) showed similar spectral features with a thiolate-protected Au_{25} cluster anion,²² that is, the absorption bands at around 400 nm and 700 nm and a shoulder peak at ca. 800 nm (Fig. 1). The absorption peak at around 700 nm, which is mainly derived from a Au_{13} core-to-core transition,²⁹ was slightly red-shifted from $\text{TOA}^+[\text{Au}_{25}(\text{SC}_2\text{Ph})_{18}]^-$ (682 nm) to $\text{TOA}^+[\text{Au}_{25}(\text{SPh})_{18}]^-$ (702 nm). These shifts of absorption bands were caused by the differences in the electronic effects of thiolate ligands.³⁰ By contrast, the shape of absorption bands in the higher energy region was clearly different depending on the SR ligands because of the direct contribution of protecting ligands to the electronic transitions.²⁹ The structural features of a series of Au_{25} cluster anions were compared using Au-L₃ edge XAFS measurements at 10 K with transmission mode (Fig. S6 and Table S1†). Extended XAFS (EXAFS) analysis showed that structures of all Au_{25} cluster anions employed in this work showed similar structural parameters (Table S1†). Moreover,

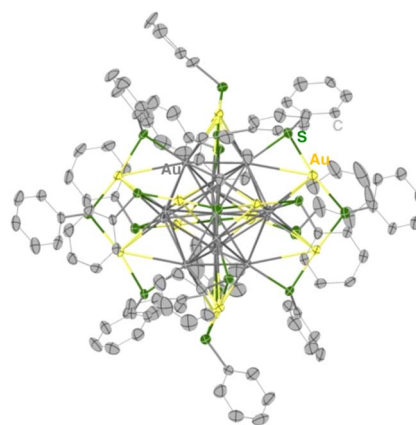


Fig. 2 A thermal ellipsoid plot (50% probability) of $\text{TOA}^+[\text{Au}_{25}(\text{SPh})_{18}]^-$. The TOA^+ cation, solvent molecules, and hydrogen atoms were omitted for clarity. Atom labels: grey: gold in the Au_{13} core, yellow: gold on the staple, green: sulfur, and light grey: carbon.



the solid-state structure of $\text{TOA}^+[\text{Au}_{25}(\text{SPh})_{18}]^-$ was clarified using single-crystal X-ray crystallographic analysis (Fig. 2 and S7†). The anionic part in $\text{TOA}^+[\text{Au}_{25}(\text{SPh})_{18}]^-$ has a Au_{13} icosahedral core (Au_{13}^{5+}) with six dimeric staple moieties ($[\text{Au}_2(\text{SR})_3]^-$), which are typical components for the Au_{25} cluster anion. The average Au–Au and Au–S bond lengths, summarized in Table S2,† were comparable to those of previously reported $\text{TOA}^+[\text{Au}_{25}(\text{SC}_2\text{Ph})_{18}]^-$.¹⁶

To determine the redox potentials of Au_{25} clusters, cyclic voltammetry (CV) and differential pulse voltammetry on a series of Au_{25} cluster anions were performed in THF containing TBAPF₆ as an electrolyte (Fig. S8†). The cyclic voltammogram of $\text{TOA}^+[\text{Au}_{25}(\text{SC}_2\text{Ph})_{18}]^-$ showed two reversible redox waves at $E_{1/2} = +0.06$ V and $+0.41$ V vs. SCE (Fig. S8a†). These two redox waves could be assigned to the redox couples of $\text{Au}_{25}^-/\text{Au}_{25}^0$ and $\text{Au}_{25}^0/\text{Au}_{25}^+$, respectively.²⁰ The first $E_{1/2}$ values were positively shifted with decreasing electron-donating abilities of thiolate ligands;³⁰ for $\text{TOA}^+[\text{Au}_{25}(\text{SC}_1\text{Ph})_{18}]^-$, the first oxidation wave was observed at $+0.16$ V vs. SCE owing to the weaker electron-donating ability of SC_1Ph than that of SC_2Ph . The largest shift of $E_{1/2}$ ($=+0.26$ V vs. SCE) was seen for $\text{TOA}^+[\text{Au}_{25}(\text{SPh})_{18}]^-$ (Fig. S8d†) with the weakest electron-donating ligands in this work. It should be noted that the $E_{1/2}$ value in the redox couple of $\text{Au}_{25}^-/\text{Au}_{25}^0$ for $\text{TOA}^+[\text{Au}_{25}(\text{SPhOMe})_{18}]^-$ ($E_{1/2} = +0.17$ V vs. SCE) is almost the same as that for $\text{TOA}^+[\text{Au}_{25}(\text{SC}_1\text{Ph})_{18}]^-$ (Table 1 and Fig. S8b, c†). As well as the redox properties of $[\text{Au}_{25}(\text{SR})_{18}]^-$, the affinity with O_2 should be one of the essential factors to determine reactivities with O_2 . The O_2 -affinities of inorganic nanomaterials would be affected by surface environments including structures of protecting ligands. Thus, the two kinds of $[\text{Au}_{25}(\text{SR})_{18}]^-$, with the same redox potentials but different surface ligands, could provide meaningful insights into the correlation between the O_2 -affinity and the reactivities of Au_{25} clusters.

Air-oxidation reactions of thiolate-protected Au_{25} clusters

Air-oxidation reactions of $\text{TOA}^+[\text{Au}_{25}(\text{SR})_{18}]^-$ were monitored by UV-vis spectroscopic measurements. First, we evaluated the stability of $\text{TOA}^+[\text{Au}_{25}(\text{SR})_{18}]^-$ (0.010 mM) in air-saturated THF at 298 K for 24 h (Fig. S9†). The lack of spectroscopic changes indicates that all $\text{TOA}^+[\text{Au}_{25}(\text{SR})_{18}]^-$ are highly stable in the absence of any proton sources. Jin and co-workers reported photo-mediated oxidation reactions of $[\text{Au}_{25}(\text{SC}_2\text{Ph})_{18}]^-$ under ambient light exposure,^{13d} but such oxidation reactions were not observed in our reaction system. Thus, the light irradiation from the UV-vis spectroscopic device could not induce the

photo-induced oxidation reaction and we have excluded the light-mediated effect from our reaction system. By contrast, in the presence of a Brønsted acid like trifluoroacetic acid (TFA, 0.25 mM), the absorption at 445 nm and around 800 nm of $\text{TOA}^+[\text{Au}_{25}(\text{SC}_2\text{Ph})_{18}]^-$ slightly decreased and a new absorption band at around 630 nm appeared (Fig. 3a). In addition, the absorption peak at around 400 nm became sharper. Such spectral change was also observed even in the presence of a small amount of TFA (0.050 mM, Fig. S10†). The UV-vis absorption feature of the final product indicates the formation of $[\text{Au}_{25}(\text{SC}_2\text{Ph})_{18}]^0$, a one-electron oxidized product of $[\text{Au}_{25}(\text{SC}_2\text{Ph})_{18}]^-$ (eqn (1)).²² The formation of $[\text{Au}_{25}(\text{SC}_2\text{Ph})_{18}]^0$ was also confirmed by ¹H NMR (Fig. S11†) and CV measurements of $[\text{Au}_{25}(\text{SC}_2\text{Ph})_{18}]^-$ (Fig. S12†). In the ¹H NMR spectrum, air-oxidation of $\text{TOA}^+[\text{Au}_{25}(\text{SC}_2\text{Ph})_{18}]^-$ in THF-*d*₈ gave a new peak at 5.17 ppm (Fig. S11a and b†), which was in good agreement with that from $[\text{Au}_{25}(\text{SC}_2\text{Ph})_{18}]^0$ (Fig. S11c†), supporting the formation of an one-electron-oxidized Au_{25} cluster. In the electrochemical measurements on $\text{TOA}^+[\text{Au}_{25}(\text{SC}_2\text{Ph})_{18}]^-$, the open circuit potential (OCP) was determined to be -0.03 V vs. SCE in the absence of TFA, which was more negative than $E_{1/2}$ ($\text{Au}_{25}^-/\text{Au}_{25}^0$) of $[\text{Au}_{25}(\text{SC}_2\text{Ph})_{18}]^-$ ($+0.06$ V vs. SCE). Upon addition of TFA, OCP shifted to $+0.21$ V vs. SCE, which was positioned between $E_{1/2}$ ($\text{Au}_{25}^-/\text{Au}_{25}^0$) and $E_{1/2}$ ($\text{Au}_{25}^0/\text{Au}_{25}^+$). Moreover, the negative potential sweep from $+0.21$ V showed a clear reduction wave assigned with the reduction of

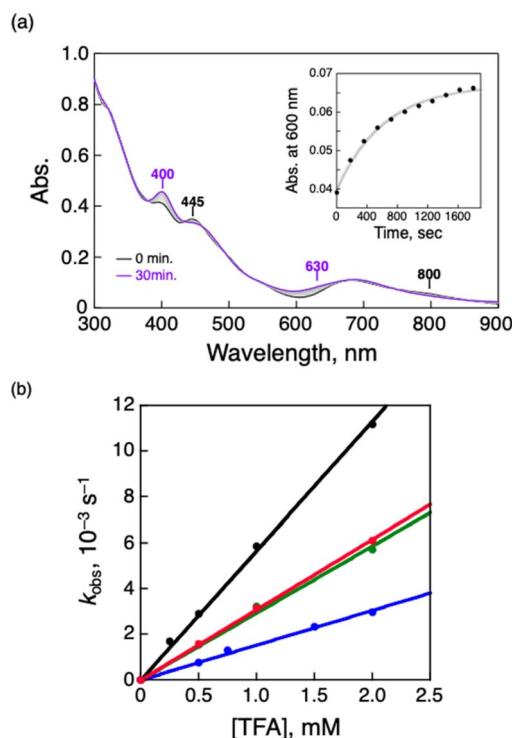


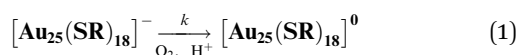
Fig. 3 (a) UV-vis spectral change of $\text{TOA}^+[\text{Au}_{25}(\text{SC}_2\text{Ph})_{18}]^-$ (0.010 mM) in air-saturated THF containing TFA (0.25 mM) at 298 K. Inset: the time profile of absorbance at 600 nm. (b) [TFA] dependence of k_{obs} in the air-oxidation reaction of $\text{TOA}^+[\text{Au}_{25}(\text{SR})_{18}]^-$ in air-saturated THF at 298 K. SR = SC_2Ph (black), SC_1Ph (green), SPhOMe (red) and SPh (blue). $[\text{O}_2] = 2.2$ mM.³¹

Table 1 Summary of redox potentials of $\text{TOA}^+[\text{Au}_{25}(\text{SR})_{18}]^-$ in THF containing 0.1 M TBAPF₆ under Ar

| SR | $E_{1/2}$ ($\text{Au}_{25}^-/\text{Au}_{25}^0$) V, vs. SCE | $E_{1/2}$ ($\text{Au}_{25}^0/\text{Au}_{25}^+$) V, vs. SCE |
|-------------------------|--|--|
| SC₂Ph | +0.06 | +0.41 |
| SC₁Ph | +0.16 | +0.50 |
| SPhOMe | +0.17 | +0.41 |
| SPh | +0.26 | +0.54 |



$[\text{Au}_{25}(\text{SC}_2\text{Ph})_{18}]^0$ to $[\text{Au}_{25}(\text{SC}_2\text{Ph})_{18}]^-$. This electrochemical evidence strongly supports the formation of the neutral Au_{25} cluster. The resulting $[\text{Au}_{25}(\text{SC}_2\text{Ph})_{18}]^0$ formed under UV-vis spectroscopic conditions could be reduced to $[\text{Au}_{25}(\text{SC}_2\text{Ph})_{18}]^-$ quantitatively (Fig. S13†) by reductants such as sodium borohydride (NaBH_4). The reversible behaviour of $\text{Au}_{25}^-/\text{Au}_{25}^0$ conversion was also observed even at a high TFA concentration (10 mM, Fig. S14†). This complete reversibility indicates that no side reactions such as decompositions of Au_{25} clusters occur, suggesting that $[\text{Au}_{25}(\text{SC}_2\text{Ph})_{18}]^-$ is desirable as a highly durable redox catalyst.



$$\begin{aligned} d[\text{Au}_{25}(\text{SR})_{18}]/dt &= k_{\text{obs}}[\text{Au}_{25}(\text{SR})_{18}]^- \\ &= k[\text{TFA}][[\text{Au}_{25}(\text{SR})_{18}]^-] \end{aligned} \quad (2)$$

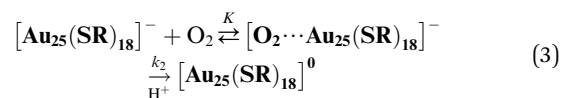
To perform the kinetic analysis in the formation of $[\text{Au}_{25}(\text{SC}_2\text{Ph})_{18}]^0$, the pseudo-first-order rate constant (k_{obs}) was determined to be $(1.6 \pm 0.1) \times 10^{-3} \text{ s}^{-1}$ at 298 K from the time course of the UV-vis spectral change at 600 nm (Fig. 3a, inset). A linear correlation was observed between the TFA concentration and k_{obs} (Fig. 3b, black), indicating that only one proton was involved in the oxidation reaction. The second-order rate constant (k in eqn (1) and (2)) could be determined to be $(5.65 \pm 0.06) \text{ M}^{-1} \text{ s}^{-1}$ from the slope. It should be noted that no oxidation reaction of $[\text{Au}_{25}(\text{SC}_2\text{Ph})_{18}]^-$ occurred in deaerated THF (Fig. S15†). Therefore, O_2 should be an oxidant for $[\text{Au}_{25}(\text{SC}_2\text{Ph})_{18}]^-$ in this reaction system. In addition, no change in optical properties of $[\text{Au}_{25}(\text{SC}_2\text{Ph})_{18}]^-$ upon addition of TFA under the degassed conditions suggests no interaction between the Au_{25} cluster and TFA (Fig. S15†). Therefore, TFA should play a role in acceleration of Au_{25} cluster air-oxidation, namely O_2 reduction through PCET, in which an electron transfer from $[\text{Au}_{25}(\text{SC}_2\text{Ph})_{18}]^-$ to O_2 and a proton comes from a Brønsted acid.²⁴ Other $\text{TOA}^+[\text{Au}_{25}(\text{SR})_{18}]^-$ ($\text{SR} = \text{SC}_1\text{Ph}$, SPh and SPhOMe) were also oxidized to form corresponding neutral $[\text{Au}_{25}(\text{SR})_{18}]^0$ in air-saturated THF containing TFA, as observed by the UV-vis spectral change (Fig. S16†). In addition, each $[\text{Au}_{25}(\text{SR})_{18}]^0$ could be fully recovered to the corresponding anionic species by the addition of NaBH_4 , indicating high durability of these $\text{Au}_{25}^-/\text{Au}_{25}^0$ redox reaction systems (Fig. S17†). Kinetic analyses were performed to determine k values (Fig. 3b), which are

Table 2 Summary of rate constants (k and k_2) and equilibrium constants (K) in the air oxidation of $\text{TOA}^+[\text{Au}_{25}(\text{SR})_{18}]^-$ in THF in the presence of TFA^a

| SR | $k, \text{M}^{-1} \text{s}^{-1}$ | k_2, s^{-1} | K, mM^{-1} |
|------------------------|----------------------------------|----------------------|---------------------|
| SC_2Ph | 5.65 ± 0.06 | 9.9 ± 0.3 | 0.20 ± 0.01 |
| SC_1Ph | 2.93 ± 0.08 | 4.2 ± 0.1 | 0.26 ± 0.03 |
| SPhOMe | 3.19 ± 0.01 | 3.67 ± 0.03 | 0.34 ± 0.01 |
| SPh | 1.51 ± 0.02 | 1.35 ± 0.01 | 0.55 ± 0.01 |

^a At 298 K. $[\text{Au}_{25}(\text{SR})_{18}]^- = 0.010 \text{ mM}$.

summarized in Table 2. The oxidation reaction of $[\text{Au}_{25}(\text{SC}_2\text{Ph})_{18}]^-$ with the lowest one-electron oxidation potential (+0.06 V vs. SCE, Table 1) showed the highest k value, whereas the lowest k value was confirmed in $\text{TOA}^+[\text{Au}_{25}(\text{SPh})_{18}]^-$ with the highest $E_{1/2}$ among $\text{TOA}^+[\text{Au}_{25}(\text{SR})_{18}]^-$ in this work. The reactivities of $\text{TOA}^+[\text{Au}_{25}(\text{SC}_1\text{Ph})_{18}]^-$ and $\text{TOA}^+[\text{Au}_{25}(\text{SPhOMe})_{18}]^-$ were almost the same despite the different types of SR moieties (benzylic and aromatic thiolate, respectively). Considering the similar $E_{1/2}$ values between $\text{TOA}^+[\text{Au}_{25}(\text{SC}_1\text{Ph})_{18}]^-$ and $\text{TOA}^+[\text{Au}_{25}(\text{SPhOMe})_{18}]^-$ (Table 1), the redox potential of $\text{TOA}^+[\text{Au}_{25}(\text{SR})_{18}]^-$ should be one of the main controlling factors to determine the reactivities with O_2 .



$$k_{\text{obs}} = \frac{k_2 K [\text{O}_2]}{1 + K [\text{O}_2]} \quad (4)$$

Häkkinen and co-workers demonstrated that small molecules such as O_2 were able to access the surface of ligand-protected AuNCs, which would play an important role in small molecule activation.³² Then, to examine the interaction of the surface of $[\text{Au}_{25}(\text{SR})_{18}]^-$ with O_2 during air-oxidation reactions, kinetic analyses were performed by changing the concentration of O_2 in THF (Fig. 4). The pseudo-first-order rate constants (k_{obs}) of the air-oxidation reaction of $\text{TOA}^+[\text{Au}_{25}(\text{SR})_{18}]^-$ showed saturation behaviour on increasing the concentration of O_2 , suggesting the existence of a pre-equilibrium between $\text{TOA}^+[\text{Au}_{25}(\text{SR})_{18}]^-$ and O_2 (eqn (3)). Based on eqn (4),³³ pre-equilibrium constants (K), namely O_2 binding constants with Au_{25} cluster anions, and second-order rate constants (k_2) were determined and are summarized in Table 2. In the case of $\text{TOA}^+[\text{Au}_{25}(\text{SC}_2\text{Ph})_{18}]^-$, k_2 and K were $(9.9 \pm 0.3) \text{ s}^{-1}$ and $(0.20 \pm 0.01) \text{ mM}^{-1}$ at $[\text{TFA}] = 0.50 \text{ mM}$, respectively. When changing the concentration of TFA to 2.0 mM, the K value was retained ($0.18 \pm 0.04 \text{ mM}^{-1}$), whereas the k_2 value increased ($(44 \pm 4) \text{ s}^{-1}$) (Fig. S18†). No influence of

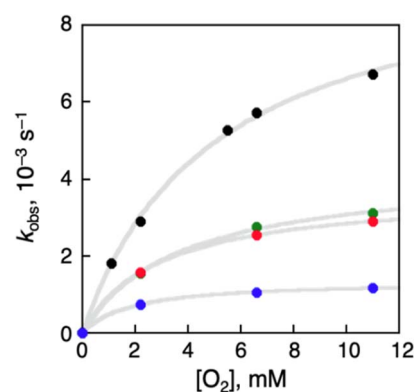


Fig. 4 $[\text{O}_2]$ dependence of k_{obs} in oxidation reactions of $\text{TOA}^+[\text{Au}_{25}(\text{SR})_{18}]^-$ in THF ($[\text{TFA}] = 0.50 \text{ mM}$) at 298 K. SR = SC_2Ph (black), SC_1Ph (green), SPhOMe (red) and SPh (blue).



the acid concentration on the O₂ binding constant suggests that protons are not involved in the pre-equilibrium between the Au₂₅ cluster and O₂ (eqn (3)). The highest O₂ binding constant (0.55 ± 0.01 mM⁻¹) was observed in the air-oxidation reaction of TOA⁺[Au₂₅(SPh)₁₈]⁻, whereas TOA⁺[Au₂₅(SC₂Ph)₁₈]⁻ showed the lowest O₂-binding properties (0.20 ± 0.01 mM⁻¹). In other words, Au₂₅ cluster anions protected by rigid aromatic thiolate ligands showed higher O₂ binding constants than those with flexible aliphatic thiolate ligands. The affinity of O₂ would be regulated by the electronic effects and/or the steric effects of R moieties of thiolate ligands. In mononuclear metal complexes, more electron-donating ligands increased the O₂-binding constants,³⁴ whereas an opposite tendency was observed in our system, in that more electron-donating ligands such as SC₂Ph gave reduced *K* values. This difference between MNCs and transition metal complexes would be caused by the binding position of O₂: in mononuclear metal complexes, because both the O₂-binding and the redox reactions generally take place at the same sites, namely the metal centres (Fig. 5a), the affinity of O₂ should be affected by the electronic states of metal centres. Although experimental evidence for O₂ binding sites is insufficient due to the weak electronic interaction between O₂ and AuNCs^{13d} and further spectral and structural analyses for O₂-bound Au₂₅ clusters are needed, some theoretical reports discussed that O₂ would bind with the gold atom of staple Au₂(SR)₃ moieties of [Au₂₅(SR)₁₈]⁻ in an end-on coordinating fashion rather than the Au₁₃ icosahedral core.^{13d,17d} It should be noted that the one-electron oxidation of [Au₂₅(SR)₁₈]⁻ occurs at the Au₁₃ core, not at the staple Au₂(SR)₃ units.^{19b} Therefore, we could think that the O₂-binding and the redox sites are different in the ligand-protected MNCs, suggesting almost no electronic effects on the O₂ affinity (Fig. 5b). To evaluate the steric effects of protecting ligands, ligand flexibility such as free rotation of alkyl chains should also be considered.³⁵ We compared the half cone angles (*θ*) of [Au₂₅(SC₂Ph)₁₈]⁻ and [Au₂₅(SPh)₁₈]⁻ based on the atomic structures revealed by X-ray analysis. The *θ* value is defined as the averaged C–Au–S angle, where C is the carbon atom at the *ortho*-position of the phenyl ring of SC₂Ph or SPh ligands (Fig. S19[†]). The *θ* (63.2°) for [Au₂₅(SC₂Ph)₁₈]⁻ is larger

than that for [Au₂₅(SPh)₁₈]⁻ (50.3°), indicating the sterically more crowded environment on the surface of [Au₂₅(SC₂Ph)₁₈]⁻. Based on the above discussion, it would be reasonable to explain that the steric effects of thiolate moieties, their bulkiness or flexibility, are dominant factors in determining the O₂-affinity with a Au₂₅ cluster anion. This conclusion suggests that O₂ would be favourably bound at a less steric gold(I) ion at the staple moiety rather than at sterically crowded metal-core gold atoms, which does not contradict with the theoretical analysis.^{13d,17d}

Finally, we considered the controlling factors in determining the reactivities of Au₂₅ clusters. As seen in the comparison of the kinetic parameters (*K* and *k*₂) of [Au₂₅(SC₂Ph)₁₈]⁻ with those of [Au₂₅(SPh)₁₈]⁻ (Table 2), the electronic effects of Au₂₅ clusters, evaluated using redox potentials (*E*_{1/2}), are a dominant factor in regulating the reaction with O₂. Indeed, a linear relationship was observed between *k*₂ values and *E*_{1/2} (Au₂₅⁻/Au₂₅⁰), as shown in Fig. S20.[†] However, interestingly, a different aspect could be seen when the influences of O₂ affinity on the reactivities were extracted from the kinetic parameters of TOA⁺[Au₂₅(SC₁Ph)₁₈]⁻ and TOA⁺[Au₂₅(SPhOMe)₁₈]⁻: a higher *K* value (0.34 ± 0.01 mM⁻¹) was observed in TOA⁺[Au₂₅(SPhOMe)₁₈]⁻, whereas the *k*₂ value of TOA⁺[Au₂₅(SPhOMe)₁₈]⁻ (3.67 ± 0.03 s⁻¹) was slightly lower than that of TOA⁺[Au₂₅(SC₁Ph)₁₈]⁻ (4.2 ± 0.1 s⁻¹), resulting in comparable reactivities of these two Au₂₅ clusters. Thus, the steric effects of protecting ligands could also contribute to tuning the reactivities of the Au₂₅ clusters against O₂. For *ca.* 3 nm gold nanoparticles, the reactivities with O₂ were simply correlated with O₂-binding constants in pre-equilibrium,^{12c} which were regulated using the accessibility to active sites. In contrast, the oxidation reactivities of [Au₂₅(SR)₁₈]⁻ with O₂ could be controlled over both steric and electronic effects. This dual effect on the reactivity enables us to construct finely tunable reaction systems by protecting ligand design, which should be important for precisely controlled catalytic systems based on inorganic nanomaterials.

Conclusions

We have compared the air-oxidation reactivities of a series of thiolate-protected Au₂₅ nanoclusters bearing different ligands. Kinetic analysis for the oxidation of Au₂₅⁻ to Au₂₅⁰ has quantitatively revealed that the O₂-affinity was regulated by the accessibility of surface gold atoms surrounded by protecting ligands, similar to other inorganic nanomaterials. On the other hand, the total reactivities with O₂ can also be tuned by the electronic states of Au₂₅ clusters such as transition metal complexes. This duality in controlling factors for reactivities allows us to construct precisely controlled reaction systems based on metal nanoclusters, which can be achieved by the rational design of protecting ligands. These results shed new light on ligand-protected MNCs with sizes of less than 2 nm to construct finely tunable reaction systems, in contrast to the case of reaction systems based on larger MNPs. Ligand designs, considering ligand–ligand or ligand–substrate interactions, should be effective for more precise control over the reactivities of MNCs.

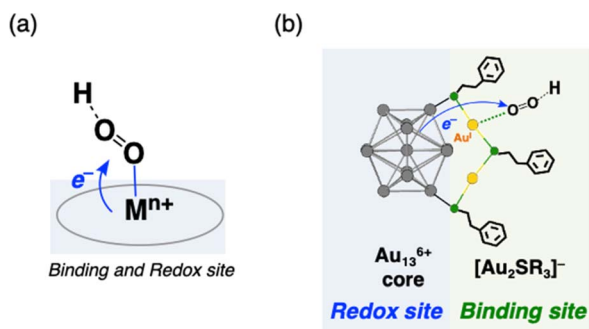


Fig. 5 Schematic illustrations of the interaction and reduction of O₂ with (a) transition metal complexes and (b) [Au₂₅(SR)₁₈]⁻ through PCET. In (b), only one staple moiety (Au₂SR₃ unit) is shown for clarity. Atom labels: grey: gold in the Au₁₃ core, yellow: gold on the staple, and green: sulfur.



Data availability

Additional experimental data supporting this article are included in the ESI.† Reasonable requests for additional information can be made to the corresponding authors.

Author contributions

W. S. designed the research, performed the synthesis and characterisation and wrote the manuscript. R. T. performed EXAFS measurements using the synchrotron. Y. M. and N. T. performed single crystal X-ray diffraction measurement and analysis. S. X. contributed to the discussion and editing the manuscript. T. T. supervised the research. All authors have approved the manuscript.

Conflicts of interest

There are no conflicts to declare.

Acknowledgements

XAFS measurements were performed at the BL01B1 of SPring-8 with the approval of the Japan Synchrotron Radiation Research Institute (JASRI). This work was financially supported by the MEXT/Japan Society for the Promotion of Science (JSPS), KAKENHI, for Scientific Research (S) (grant no. JP19H05634 and JP24H00053) (T. T.), a JSPS Research Fellowship (grant no. 20J01921), JSPS KAKENHI for Early-Career Scientists (grant no. JP23K13765), International Collaboration Research Project of the Institute for Chemical Research, Kyoto University (grant no. 2024-119), and the Tokuyama Science Foundation (W. S.). We thank Ian McNaught, PhD, from Edanz (<https://jp.edanz.com/ac>) for editing a draft of this manuscript.

References

- (a) M. L. Peigs, C. F. Wise, D. J. Martin and J. M. Mayer, *Chem. Rev.*, 2018, **118**, 2340–2391; (b) H. Sterckx, B. Morel and B. U. W. Maes, *Angew. Chem., Int. Ed.*, 2019, **58**, 7946–7970.
- (a) D. J. Martin, C. F. Wise, M. L. Peigs and J. M. Mayer, *Acc. Chem. Res.*, 2020, **53**, 1056–1065; (b) A. Rana, Y.-M. Lee, X. Li, R. Cao, S. Fukuzumi and W. Nam, *ACS Catal.*, 2021, **11**(5), 3073–3083; (c) S. Fukuzumi, L. Tahsini, Y.-M. Lee, K. Ohkubo, W. Nam and K. D. Karlin, *J. Am. Chem. Soc.*, 2012, **134**, 7025–7035.
- (a) I. Hatay, B. Su, M. A. Méndez, C. Corminboeuf, T. Khoury, C. P. Gross, M. Bourdillon, M. Meyer, J.-M. Barbe, M. Ersoz, S. Zálší, Z. Samec and H. H. Girault, *J. Am. Chem. Soc.*, 2010, **132**, 13733–13741; (b) K. Mase, K. Ohkubo, Z. Xue, H. Yamada and S. Fukuzumi, *Chem. Sci.*, 2015, **6**, 6496–6504; (c) E. Aoki, W. Suzuki, H. Kotani, T. Ishizuka, H. Sakai, T. Hasobe and T. Kojima, *Chem. Commun.*, 2019, **55**, 4925–4928.
- (a) Y. Zhang, X. Cui, F. Shi and Y. Deng, *Chem. Rev.*, 2012, **112**, 2467–2505; (b) C. Xie, Z. Niu, D. Kim, M. Li and P. Yang, *Chem. Rev.*, 2020, **120**, 1184–1249.
- M. Haruta, T. Kobayashi, H. Sano and N. Yamada, *Chem. Lett.*, 1987, 405–408.
- (a) M. K. Carpenter, T. E. Moylan, R. S. Kukreja, M. H. Atwan and M. M. Tessema, *J. Am. Chem. Soc.*, 2012, **134**, 8535–8542; (b) M. Daka, M. Ferrara, M. Bevilacqua, P. Pengo, P. Rajak, R. Ciancio, T. Montini, L. Pasquato and P. Fornasiero, *ACS Appl. Nano Mater.*, 2022, **5**, 4710–4720.
- (a) Y. Du, H. Sheng, D. Astruc and M. Zhu, *Chem. Rev.*, 2020, **120**, 526–622; (b) R. Jin, G. Li, S. Sharma, Y. Li and X. Du, *Chem. Rev.*, 2021, **121**, 567–648.
- (a) Y. Zhu, H. Qian, M. Zhu and R. Jin, *Adv. Mater.*, 2010, **22**, 1915–1920; (b) K. Harano, S. Takano and T. Tsukuda, *Chem. Commun.*, 2019, **55**, 15033–15036; (c) S. Tian, Y. Cao, T. Chen, S. Zang and J. Xie, *Chem. Commun.*, 2020, **56**, 1163–1174; (d) S. Zhuang, D. Chen, W.-P. Ng, D. Liu, L.-J. Liu, M.-Y. Sun, T. Nawaz, X. Wu, Y. Zhang, Z. Li, Y.-L. Huang, J. Yang and J. He, *JACS Au*, 2022, **2**, 2617–2626.
- (a) H. Tsunoyama, A. Ohnuma, K. Takahashi, A. Velloth, M. Ehara, N. Ichikuni, M. Tabuchi and A. Nakajima, *Chem. Commun.*, 2019, **55**, 12603–12606; (b) T. Kawawaki, N. Shimizu, K. Funai, Y. Mitomi, S. Hossain, S. Kikkawa, D. J. Osborn, S. Yamazoe, G. F. Metha and Y. Negishi, *Nanoscale*, 2021, **13**, 14679–14687.
- (a) R. R. Jacobson, Z. Tyeklar, A. Farooq, K. D. Karlin, S. Liu and J. Zubieta, *J. Am. Chem. Soc.*, 1988, **110**, 3690–3692; (b) T. Chishiro, Y. Shimazaki, F. Tani, Y. Tachi, Y. Naruta, S. Karasawa, S. Hayami and Y. Maeda, *Angew. Chem., Int. Ed.*, 2003, **42**, 2788–2791; (c) J. Cho, R. Sarangi, H. Y. Kang, J. Y. Lee, M. Kubo, T. Ogura, E. I. Solomon and W. Nam, *J. Am. Chem. Soc.*, 2010, **132**, 16977–16986.
- (a) H. Kotani, T. Yagi, T. Ishizuka and T. Kojima, *Chem. Commun.*, 2015, **51**, 13385–13388; (b) C. W. Anson, S. Ghosh, S. Hammes-Schiffer and S. S. Stahl, *J. Am. Chem. Soc.*, 2016, **138**, 4186–4193; (c) W. Suzuki, H. Kotani, T. Ishizuka and T. Kojima, *J. Am. Chem. Soc.*, 2019, **141**(14), 5987–5994; (d) W. Suzuki, H. Kotani, T. Ishizuka and T. Kojima, *Chem.–Eur. J.*, 2020, **26**(46), 10480–10486.
- (a) A. Abad, A. Corma and H. García, *Chem.–Eur. J.*, 2008, **14**, 212–222; (b) C. Shang and Z.-P. Liu, *J. Am. Chem. Soc.*, 2011, **133**, 9938–9947; (c) C. G. Long, J. D. Gilbertson, G. Vijayaraghavan, K. J. Stevenson, C. J. Pursell and B. D. Chandler, *J. Am. Chem. Soc.*, 2008, **130**, 10103–10115.
- (a) A. Sanchez, S. Abbet, U. Heiz, W.-D. Schneider, H. Häkkinen, R. N. Barnett and U. Landman, *J. Phys. Chem. A*, 1999, **103**, 9578; (b) H. Tsunoyama, N. Ichikuni, H. Sakurai and T. Tsukuda, *J. Am. Chem. Soc.*, 2009, **131**, 7086–7093; (c) Y. Zhu, H. Qian and R. Jin, *Chem.–Eur. J.*, 2010, **16**, 11455–11462; (d) D. R. Kauffman, D. Alfonso, C. Matranga, G. Li and R. Jin, *J. Phys. Chem. Lett.*, 2013, **4**, 195–202; (e) Z. Wu, G. Hu, D. Jiang, D. R. Mullins, Q.-F. Zhang, L. F. Allard Jr, L.-S. Wang and S. H. Overbury, *Nano Lett.*, 2016, **16**, 6550–6567; (f) D. A. Pichugina, N. A. Nikitina and N. E. Kuzmenko, *J. Phys. Chem. C*, 2020, **124**, 3080–3086.
- (a) Y. Negishi, T. Nakazaki, S. Malola, S. Takano, Y. Niihori, W. Kurashige, S. Yamazoe, T. Tsukuda and H. Häkkinen, *J. Am. Chem. Soc.*, 2015, **137**, 1206–1212; (b) S. Yamazoe,



- S. Takano, W. Kurashige, T. Yokoyama, K. Nitta, Y. Negishi and T. Tsukuda, *Nat. Commun.*, 2016, **7**, 10414; (c) I. Chakraborty and T. Pradeep, *Chem. Rev.*, 2017, **117**, 8208–8271.
- 15 (a) G. Li, H. Abroshan, C. Liu, S. Zhuo, Z. Li, Y. Xie, H. J. Kim, N. L. Rosi and R. Jin, *ACS Nano*, 2016, **10**, 7998–8005; (b) R. R. Nasaruddin, Q. Yao, T. Chen, M. J. Hülsey, N. Yan and J. Xie, *Nanoscale*, 2018, **10**, 23113–23121; (c) Q. Yao, Z. Wu, Z. Liu, Y. Lin, X. Yuan and J. Hie, *Chem. Sci.*, 2021, **12**, 99–127; (d) H. Shan, J. Shi, T. Chen, Y. Cao, Q. Yao, H. An, Z. Yang, Z. Wu, Z. Jiang and J. Xie, *ACS Nano*, 2023, **17**, 2368–2377.
- 16 (a) M. Zhu, C. M. Aikens, F. J. Hollander, G. C. Schatz and R. Jin, *J. Am. Chem. Soc.*, 2008, **130**, 5883–5885; (b) M. W. Heaven, A. Dass, P. S. White, K. M. Holt and R. W. Murray, *J. Am. Chem. Soc.*, 2008, **130**, 3754–3755.
- 17 (a) Y. Lu, Y. Jiang, X. Gao and W. Chen, *Chem. Commun.*, 2014, **50**, 8464–8467; (b) B. Kumar, T. Kawawaki, N. Shimizu, Y. Imai, D. Suzuki, S. Hossain, L. V. Nair and Y. Negishi, *Nanoscale*, 2020, **12**, 9969–9979; (c) W. Chen and S. Chen, *Angew. Chem., Int. Ed.*, 2009, **48**, 4386–4389; (d) F. Sun, C. Deng, S. Tian and Q. Tang, *ACS Catal.*, 2021, **11**, 7957–7969.
- 18 Y. Saito, Y. Shichibu and K. Konishi, *Nanoscale*, 2021, **13**, 9971–9977.
- 19 (a) T. A. Dreier, O. A. Wong and C. J. Aikens, *Chem. Commun.*, 2015, **51**, 1240–1243; (b) M. Zhu, C. M. Aikens, M. P. Hendrich, R. Gupta, H. Qian, G. C. Schatz and R. Jin, *J. Am. Chem. Soc.*, 2009, **131**, 2490–2492.
- 20 (a) S. Antonello, A. H. Holm, E. Instuli and F. Maran, *J. Am. Chem. Soc.*, 2007, **129**, 9836–9837; (b) S. Antonello, N. V. Perera, M. Ruzzi, J. A. Gascón and F. Maran, *J. Am. Chem. Soc.*, 2013, **135**, 15585–15594; (c) S. Antonello, G. Arrigoni, T. Dainese, M. De Nardi, G. Parisio, L. Perotti, A. René, A. Venzo and F. Maran, *ACS Nano*, 2014, **8**, 2788–2795; (d) K. Kwak and D. Lee, *Acc. Chem. Res.*, 2019, **52**, 12–22.
- 21 S. Bhat, R. Pradeep, N. Ananya, P. Chakraborty, G. Paramasivam, R. R. J. Methikkalam, A. Nag, G. Natarajan and T. Pradeep, *J. Phys. Chem. C*, 2018, **122**, 19455–19462.
- 22 M. Zhu, W. T. Eckenhoff, T. Pintauer and R. Jin, *J. Phys. Chem. C*, 2008, **112**, 14221–14224.
- 23 (a) X. Yuan, N. Goswami, W. Chen, Q. Yao and J. Xie, *Chem. Commun.*, 2016, **52**, 5234–5237; (b) Z. Lei, J.-J. Li, Z.-A. Nan, Z.-G. Jiang and Q.-M. Wang, *Angew. Chem., Int. Ed.*, 2021, **60**, 14415–14419; (c) W. Suzuki, R. Takahata, Y. Chiga, S. Kikkawa, S. Yamazoe, Y. Mizuhata, N. Tokitoh and T. Teranishi, *J. Am. Chem. Soc.*, 2022, **144**, 12310–12320.
- 24 (a) D. R. Weinberg, C. J. Gagliardi, J. F. Hull, C. F. Murphy, C. A. Kent, B. C. Westlake, A. Paul, D. H. Ess, D. G. McCafferty and T. J. Meyer, *Chem. Rev.*, 2012, **112**, 4016–4093; (b) S. Fukuzumi, Y.-M. Lee and W. Nam, *ChemCatChem*, 2018, **10**, 9–28.
- 25 W. Suzuki, H. Kotani, T. Ishizuka and T. Kojima, *Chem.–Eur. J.*, 2020, **26**, 10480–10486.
- 26 K. Mase, K. Ohkubo and S. Fukuzumi, *J. Am. Chem. Soc.*, 2013, **135**, 2800–2808.
- 27 J. F. Parker, J. E. F. Weaver, F. McCallum, C. A. Fields-Zinna and R. W. Murray, *Langmuir*, 2010, **26**(16), 13650–13654.
- 28 M. P. Maman, A. S. Nair, A. M. A. H. Nazeer, B. Pathak and S. Mandal, *J. Phys. Chem. Lett.*, 2020, **11**, 10052.
- 29 C. M. Aikens, *J. Phys. Chem. Lett.*, 2010, **1**, 2594–2599.
- 30 (a) R. Guo and R. W. Murray, *J. Am. Chem. Soc.*, 2005, **127**, 12140–12143; (b) Z. Liu, Y. Li, E. Kahng, S. Xue, X. Du, S. Li and R. Jin, *ACS Nano*, 2022, **16**, 18448–18458.
- 31 D. Das, Y.-M. Lee, K. Ohkubo, W. Nam, K. D. Karlin and S. Fukuzumi, *J. Am. Chem. Soc.*, 2013, **135**, 2825–2834.
- 32 (a) X. Chen and H. Häkkinen, *J. Am. Chem. Soc.*, 2013, **135**, 12944–12947; (b) O. Lopez-Acevedo, K. A. Kacprzak, J. Akola and H. Häkkinen, *Nat. Chem.*, 2010, **2**, 329–334.
- 33 T. Ishizuka, S. Ohzu, H. Kotani, Y. Shiota, K. Yoshizawa and T. Kojima, *Chem. Sci.*, 2014, **5**, 1429–1436.
- 34 M. L. Pegis, B. A. McKeown, N. Kumar, K. Lang, D. J. Wasylenko, X. P. Zhang, S. Rauegi and J. M. Mayer, *ACS Cent. Sci.*, 2016, **2**, 850–856.
- 35 J. A. Bilbrey, A. H. Kazez, J. Locklin and W. D. Allen, *J. Comput. Chem.*, 2013, **34**, 1189–1197.

